2011 IEEE International Conference on Rehabilitation Robotics
Rehab Week Zurich, ETH Zurich Science City, Switzerland, June 29 - July 1, 2011

Estimation of IMU and MARG orientation using a gradient descent algorithm

Sebastian O.H. Madgwick, Andrew J.L. Harrison, Ravi Vaidyanathan

***Abstract*—This paper presents a novel orientation algorithm designed to support a computationally efficient, wearable inertial human motion tracking system for rehabilitation applications. It is applicable to inertial measurement units (IMUs) consisting of tri-axis gyroscopes and accelerometers, and magnetic angular rate and gravity (MARG) sensor arrays that also include tri-axis magnetometers. The MARG implementation incorporates magnetic distortion compensation. The algorithm uses a quaternion representation, allowing accelerometer and magnetometer data to be used in an analytically derived and optimised gradient descent algorithm to compute the direction of the gyroscope measurement error as a quaternion derivative. Performance has been evaluated empirically using a commercially available orientation sensor and reference measurements of orientation obtained using an optical measurement system. Performance was also benchmarked against the propriety Kalman-based algorithm of orientation sensor. Results indicate the algorithm achieves levels of accuracy matching that of the Kalman based algorithm; $< 0.8^\circ$ static RMS error, $< 1.7^\circ$ dynamic RMS error. The implications of the low computational load and ability to operate at small sampling rates significantly reduces the hardware and power necessary for wearable inertial movement tracking, enabling the creation of lightweight, inexpensive systems capable of functioning for extended periods of time.**

I. Introduction

The accurate measurement of orientation plays a critical role in a range of fields including: aerospace [1], robotics [2], [3], navigation [4], [5] and human motion analysis [6], [7] and machine interaction [8]. In rehabilitation, motion tracking is vital enabling technology, in particular for monitoring outside clinical environs; ideally, a patient's activities could be continuously monitored, and subsequently corrected. While extensive work has been performed for motion tracking for rehabilitation, an unobtrusive, wearable system capable of logging data for extended periods of time has yet to be realized. Existing systems often require a laptop or handheld PC to be carried by the subject due to the processing, data storage, and power requirements of the sensory equipment. This is not practical outside of a laboratory environment, thus detailed data may only be obtained for short periods of time for a limited range of subject's motion. More precise data representative of a subject's natural behaviour over extended periods of time (e.g. an entire day or even a week) would be of significant utility in this realm. In a recent survey, Zhoua [7], cited real time operation, wireless properties, correctness of data, and portability as major deficiencies that must be addressed to realize a clinically viable system.

Sebastian Madgwick is with the Department of Mechanical Engineering, University of Bristol, e-mail: s.madgwick@bristol.ac.uk.

Ravi Vaidyanathan is with the Department of Mechanical Engineering, University of Bristol, Queens Building, BS8 1TR and the Department of Systems Engineering at the US Naval Postgraduate School, Monterey, CA, USA, 93940. e-mail: r.vaidyanathan@bristol.ac.uk.

Andrew Harrison is with the Department of Mechanical Engineering, University of Bristol, e-mail: andrew.j.l.harrison@bristol.ac.uk.

A. Inertial Motion Tracking Systems

Whilst a variety of technologies enable the measurement of orientation, inertial based sensory systems have the advantage of being completely self contained such that the measurement entity is constrained neither in motion nor to any specific environment or location. An IMU (Inertial Measurement Unit) consists of gyroscopes and accelerometers enabling the tracking of rotational and translational movements. In order to measure in three dimensions, tri-axis sensors consisting of 3 mutually orthogonal sensitive axes are required. A MARG (Magnetic, Angular Rate, and Gravity) sensor is a hybrid IMU which incorporates a tri-axis magnetometer. An IMU alone can only measure an attitude relative to the direction of gravity which is sufficient for many applications [2], [1], [6]. MARG systems, also known as AHRS (Attitude and Heading Reference Systems) are able to provide a *complete* measurement of orientation relative to the direction of gravity and the earth's magnetic field. An orientation estimation algorithm is a fundamental component of any IMU or MARG system. It is required to fuse together the separate sensor data into a single, optimal estimate of orientation.

The Kalman filter [9] has become the accepted basis for the majority of orientation algorithms [2], [10], [11], [12] and commercial inertial orientation sensors; xsens [13], microstrain [14], VectorNav [15], Intersense [16], PNI [17] and Crossbow [18] all produce systems founded on its use. The widespread use of Kalman-based solutions are a testament to their accuracy and effectiveness, however, they have a number of disadvantages. They can be complicated to implement which is reflected by the numerous solutions seen in the subject literature [2], [10], [11], [12], [19], [20], [21], [22], [23]. The linear regression iterations, fundamental to the Kalman process, demand sampling rates which can far exceed the subject bandwidth (e.g. a sampling rate between 512 Hz [13] and 30 kHz [14] may be necessary for human motion capture applications where system portability is critical). The state relationships describing rotational kinematics in three-dimensions typically require large state vectors and an extended Kalman filter implementation [2], [12], [19] to linearise the problem.

These challenges demand a large computational load for implementation of Kalman-based solutions and provide a clear

978-1-4244-9862-8/11/$26.00 ©2011 IEEE

motivation for alternative approaches. Previous approaches to address these issues have implemented either fuzzy processing [1], [3] or frequency domain filters [24] to favour accelerometer measurements of orientation at low angular velocities and the integrated gyroscope measurements at high angular velocities. Such an approach is simple but may only be effective under limited operating conditions. Bachman *et al* [25] and Mahony *et al* [26] present separate algorithms which both employ a complementary filter process. This algorithm structure has been shown to provide effective performance at relatively little computational expense.

This paper introduces orientation estimation algorithm that is applicable to both IMU and MARG systems. The algorithm employs a quaternion representation of orientation (as in: [25], [12], [19]) to describe the coupled nature of orientations in three-dimensions and is not subject to the problematic singularities associated with an Euler angle representation. A complete derivation and empirical evaluation of the new algorithm is presented. Its performance is benchmarked against existing commercial filters and verified with optical tracking system.

II. Organisation of paper

Section III delineates the mathematical derivation of the orientation estimation algorithm, including a description of the parameterization and compensation for magnetic distortion. Section IV describes the experimental equipment used to test and verify the performance of the algorithm. Section V quantifies the experimental testing and accuracy of the algorithm and compares it to existing systems. Section VII expands briefly gives details on implementations of the system underway currently in our laboratory in human motion tracking while Section VI summarizes conclusions and contributions of this work. Throughout the paper, a notation system of leading superscripts and subscripts adopted from Craig [27] is used to denote the relative frames of orientations and vectors. A leading subscript denotes the frame being described and a leading superscript denotes the frame this is with reference to. For example, For example, ${}^{A}_{B}\hat{\boldsymbol{q}}$ describes the orientation of frame B relative to frame A and ${}^{A}\hat{\boldsymbol{v}}$ is a vector described in frame A.

III. Algorithm derivation

A. Orientation from angular rate

A tri-axis gyroscope will measure the angular rate about the x, y and z axes of the senor frame, termed ω_x, ω_y and ω_z respectively. If these parameters (in rads^{-1}) are arranged into the vector ${}^{S}\boldsymbol{\omega}$ defined by equation (1), the quaternion derivative describing rate of change of the earth frame relative to the sensor frame ${}^{S}_{E}\dot{\boldsymbol{q}}$ can be calculated [28] as equation (2). The $\otimes$ operate denotes a quaternion product and the $\hat{}$ accent denotes a normalised vector of unit length.

$$ {}^{S}\boldsymbol{\omega} = \begin{bmatrix} 0 & \omega_x & \omega_y & \omega_z \end{bmatrix} \tag{1} $$

$$ {}^{S}_{E}\dot{\boldsymbol{q}} = \frac{1}{2} {}^{S}_{E}\hat{\boldsymbol{q}} \otimes {}^{S}\boldsymbol{\omega} \tag{2} $$

The orientation of the earth frame relative to the sensor frame at time t, ${}^{E}_{S}\boldsymbol{q}_{\omega,t}$, can be computed by numerically integrating the quaternion derivative ${}^{S}_{E}\dot{\boldsymbol{q}}_{\omega,t}$ as described by equations (3) and (4), provided that initial conditions are known. In these equations, ${}^{S}\boldsymbol{\omega}_t$ is the angular rate measured at time t, Δt is the sampling period and ${}^{S}_{E}\hat{\boldsymbol{q}}_{est,t-1}$ is the previous estimate of orientation. The subscript ω indicates that the quaternion is calculated from angular rates.

$$ {}^{S}_{E}\dot{\boldsymbol{q}}_{\omega,t} = \frac{1}{2} {}^{S}_{E}\hat{\boldsymbol{q}}_{est,t-1} \otimes {}^{S}\boldsymbol{\omega}_t \tag{3} $$

$$ {}^{S}_{E}\boldsymbol{q}_{\omega,t} = {}^{S}_{E}\hat{\boldsymbol{q}}_{est,t-1} + {}^{S}_{E}\dot{\boldsymbol{q}}_{\omega,t}\Delta t \tag{4} $$

B. Orientation from a homogenous field

In the context of an orientation estimation algorithm, it will initially be assumed that an accelerometer will measure only gravity and a magnetometer will measure only the earth's magnetic field. If the direction of an earth's field is known in the earth frame, a measurement of the field's direction within the sensor frame will allow an orientation of the sensor frame relative to the earth frame to be calculated. However, for any given measurement there will not be a unique sensor orientation solution, instead there will infinite solutions represented by all those orientations achieved by the rotation the true orientation around an axis parallel with the field. A quaternion representation requires a single solution to be found. This may be achieved through the formulation of an optimisation problem where an orientation of the sensor, ${}^{S}_{E}\hat{\boldsymbol{q}}$, is found as that which aligns a predefined reference direction of the field in the earth frame, ${}^{E}\hat{\boldsymbol{d}}$, with the measured field in the sensor frame, ${}^{S}\hat{\boldsymbol{s}}$; thus solving (5) where equation (6) defines the objective function.

$$ \min_{{}^{S}_{E}\hat{\boldsymbol{q}} \in \Re^4} \boldsymbol{f}({}^{S}_{E}\hat{\boldsymbol{q}}, {}^{E}\hat{\boldsymbol{d}}, {}^{S}\hat{\boldsymbol{s}}) \tag{5} $$

$$ \boldsymbol{f}({}^{S}_{E}\hat{\boldsymbol{q}}, {}^{E}\hat{\boldsymbol{d}}, {}^{S}\hat{\boldsymbol{s}}) = {}^{S}_{E}\hat{\boldsymbol{q}}^{*} \otimes {}^{E}\hat{\boldsymbol{d}} \otimes {}^{S}_{E}\hat{\boldsymbol{q}} - {}^{S}\hat{\boldsymbol{s}} \tag{6} $$

Many optimisation algorithms exist but the gradient descent algorithm is one of the simplest to both implement and compute. Equation (7) describes the gradient descent algorithm for n iterations resulting in an orientation estimation of ${}^{S}_{E}\hat{\boldsymbol{q}}_{n+1}$ based on an 'initial guess' orientation ${}^{S}_{E}\hat{\boldsymbol{q}}_0$ and a variable step-size μ. Equation (8) computes an error direction on the solution surface defined by the objective function, $\boldsymbol{f}$, and its Jacobian, $\boldsymbol{J}$.

$$ {}^{S}_{E}\boldsymbol{q}_{k+1} = {}^{S}_{E}\hat{\boldsymbol{q}}_k - \mu \frac{\nabla \boldsymbol{f}({}^{S}_{E}\hat{\boldsymbol{q}}_k, {}^{E}\hat{\boldsymbol{d}}, {}^{S}\hat{\boldsymbol{s}})}{\left\| \nabla \boldsymbol{f}({}^{S}_{E}\hat{\boldsymbol{q}}_k, {}^{E}\hat{\boldsymbol{d}}, {}^{S}\hat{\boldsymbol{s}}) \right\|}, \ k = 0, 1, 2...n \tag{7} $$

$$ \nabla \boldsymbol{f}({}^{S}_{E}\hat{\boldsymbol{q}}_k, {}^{E}\hat{\boldsymbol{d}}, {}^{S}\hat{\boldsymbol{s}}) = \boldsymbol{J}^{T}({}^{S}_{E}\hat{\boldsymbol{q}}_k, {}^{E}\hat{\boldsymbol{d}}) \boldsymbol{f}({}^{S}_{E}\hat{\boldsymbol{q}}_k, {}^{E}\hat{\boldsymbol{d}}, {}^{S}\hat{\boldsymbol{s}}) \tag{8} $$

Equations (7) and (8) describe the general form of the algorithm applicable to a field predefined in any direction. However, if the reference direction of the field is defined to only have components within 1 or 2 of the principle axis of

the earth coordinate frame then the equations simplify. An appropriate convention would be to assume that the direction of gravity defines the vertical, z axis as shown in equation (10). Substituting ${}^{E}\hat{\boldsymbol{g}}$ and normalised accelerometer measurement ${}^{S}\hat{\boldsymbol{a}}$ for ${}^{E}\hat{\boldsymbol{d}}$ and ${}^{S}\hat{\boldsymbol{s}}$ respectively, yields the simplified objective function and Jacobian defined by equations (12) and (13).

$$ {}^{S}_{E}\hat{\boldsymbol{q}} = \begin{bmatrix} q_1 & q_2 & q_3 & q_4 \end{bmatrix} \tag{9} $$

$$ {}^{E}\hat{\boldsymbol{g}} = \begin{bmatrix} 0 & 0 & 0 & 1 \end{bmatrix} \tag{10} $$

$$ {}^{S}\hat{\boldsymbol{a}} = \begin{bmatrix} 0 & a_x & a_y & a_z \end{bmatrix} \tag{11} $$

$$ \boldsymbol{f}_g({}^{S}_{E}\hat{\boldsymbol{q}}, {}^{S}\hat{\boldsymbol{a}}) = \begin{bmatrix} 2(q_2q_4 - q_1q_3) - a_x \\ 2(q_1q_2 + q_3q_4) - a_y \\ 2(\frac{1}{2} - q_2^2 - q_3^2) - a_z \end{bmatrix} \tag{12} $$

$$ \boldsymbol{J}_g({}^{S}_{E}\hat{\boldsymbol{q}}) = \begin{bmatrix} -2q_3 & 2q_4 & -2q_1 & 2q_2 \\ 2q_2 & 2q_1 & 2q_4 & 2q_3 \\ 0 & -4q_2 & -4q_3 & 0 \end{bmatrix} \tag{13} $$

The earth's magnetic field can be considered to have components in one horizontal axis and the vertical axis; the vertical component due to the inclination of the field which is between 65° and 70° to the horizontal in the UK [29]. This can be represented by equation (14). Substituting ${}^{E}\hat{\boldsymbol{b}}$ and normalised magnetometer measurement ${}^{S}\hat{\boldsymbol{m}}$ for ${}^{E}\hat{\boldsymbol{d}}$ and ${}^{S}\hat{\boldsymbol{s}}$ respectively, yields the simplified objective function and Jacobian defined by equations (16) and (17).

$$ {}^{E}\hat{\boldsymbol{b}} = \begin{bmatrix} 0 & b_x & 0 & b_z \end{bmatrix} \tag{14} $$

$$ {}^{S}\hat{\boldsymbol{m}} = \begin{bmatrix} 0 & m_x & m_y & m_z \end{bmatrix} \tag{15} $$

$$ \boldsymbol{f}_b({}^{S}_{E}\hat{\boldsymbol{q}}, {}^{E}\hat{\boldsymbol{b}}, {}^{S}\hat{\boldsymbol{m}}) = \begin{bmatrix} 2b_x(0.5 - q_3^2 - q_4^2) + \\ 2b_x(q_2q_3 - q_1q_4) + \\ 2b_x(q_1q_3 + q_2q_4) + \\ 2b_z(q_2q_4 - q_1q_3) - m_x \\ 2b_z(q_1q_2 + q_3q_4) - m_y \\ 2b_z(0.5 - q_2^2 - q_3^2) - m_z \end{bmatrix} \tag{16} $$

$$ \boldsymbol{J}_b({}^{S}_{E}\hat{\boldsymbol{q}}, {}^{E}\hat{\boldsymbol{b}}) = \begin{bmatrix} -2b_zq_3 & 2b_zq_4 \\ -2b_xq_4 + 2b_zq_2 & 2b_xq_3 + 2b_zq_1 \\ 2b_xq_3 & 2b_xq_4 - 4b_zq_2 \\ -4b_xq_3 - 2b_zq_1 & -4b_xq_4 + 2b_zq_2 \\ 2b_xq_2 + 2b_zq_4 & -2b_xq_1 + 2b_zq_3 \\ 2b_xq_1 - 4b_zq_3 & 2b_xq_2 \end{bmatrix} \tag{17} $$

As has already been discussed, the measurement of gravity or the earth's magnetic field alone will not provide a unique orientation of the sensor. To do so, the measurements and reference directions of both fields may be combined as described by equations (18) and (19). Whereas the solution surface created by the objective functions in equations (12) and (16) have a global minimum defined by a line, the solution surface define by equation (18) has a minimum define by a single point, provided that $b_x \neq 0$.

$$ \boldsymbol{f}_{g,b}({}^{S}_{E}\hat{\boldsymbol{q}}, {}^{S}\hat{\boldsymbol{a}}, {}^{E}\hat{\boldsymbol{b}}, {}^{S}\hat{\boldsymbol{m}}) = \begin{bmatrix} \boldsymbol{f}_g({}^{S}_{E}\hat{\boldsymbol{q}}, {}^{S}\hat{\boldsymbol{a}}) \\ \boldsymbol{f}_b({}^{S}_{E}\hat{\boldsymbol{q}}, {}^{E}\hat{\boldsymbol{b}}, {}^{S}\hat{\boldsymbol{m}}) \end{bmatrix} \tag{18} $$

$$ \boldsymbol{J}_{g,b}({}^{S}_{E}\hat{\boldsymbol{q}}, {}^{E}\hat{\boldsymbol{b}}) = \begin{bmatrix} \boldsymbol{J}_g^T({}^{S}_{E}\hat{\boldsymbol{q}}) \\ \boldsymbol{J}_b^T({}^{S}_{E}\hat{\boldsymbol{q}}, {}^{E}\hat{\boldsymbol{b}}) \end{bmatrix} \tag{19} $$

A conventional approach to optimisation would require multiple iterations of equation (7) to be computed for each new orientation and corresponding senor measurements. However, it is acceptable to compute one iteration per time sample provided that the convergence rate of the estimated orientation governed by μ_t is equal or greater than the rate of change of physical orientation. Equation (20) calculates the estimated orientation ${}^{S}_{E}\boldsymbol{q}_{\nabla,t}$ computed at time t based on a previous estimate of orientation ${}^{S}_{E}\hat{\boldsymbol{q}}_{est,t-1}$ and the objective function error $\nabla\boldsymbol{f}$ defined by sensor measurements ${}^{S}\hat{\boldsymbol{a}}_t$ and ${}^{S}\hat{\boldsymbol{m}}_t$ sampled at time t. The form of $\nabla\boldsymbol{f}$ is chosen according to the sensors in use, as shown in equation (21). The subscript ∇ indicates that the quaternion is calculated using the gradient descent algorithm.

$$ {}^{S}_{E}\boldsymbol{q}_{\nabla,t} = {}^{S}_{E}\hat{\boldsymbol{q}}_{est,t-1} - \mu_t \frac{\nabla\boldsymbol{f}}{\|\nabla\boldsymbol{f}\|} \tag{20} $$

$$ \nabla\boldsymbol{f} = \begin{cases} \boldsymbol{J}_g^T({}^{S}_{E}\hat{\boldsymbol{q}}_{est,t-1})\boldsymbol{f}_g({}^{S}_{E}\hat{\boldsymbol{q}}_{est,t-1}, {}^{S}\hat{\boldsymbol{a}}_t) \\ \boldsymbol{J}_{g,b}^T({}^{S}_{E}\hat{\boldsymbol{q}}_{est,t-1}, {}^{E}\hat{\boldsymbol{b}})\boldsymbol{f}_{g,b}({}^{S}_{E}\hat{\boldsymbol{q}}_{est,t-1}, {}^{S}\hat{\boldsymbol{a}}_t, {}^{E}\hat{\boldsymbol{b}}, {}^{S}\hat{\boldsymbol{m}}_t) \end{cases} \tag{21} $$

An appropriate value of μ_t is that which ensures the convergence rate of ${}^{S}_{E}\boldsymbol{q}_{\nabla,t}$ is limited to the physical orientation rate as this avoids overshooting due an unnecessarily large step size. Therefore μ_t can be calculated as equation (22) where Δt is the sampling period, ${}^{S}_{E}\dot{\boldsymbol{q}}_{\omega,t}$ is the rate of change of orientation measured by gyroscopes and α is an augmentation of μ to account for noise in accelerometer and magnetometer measurements.

$$ \mu_t = \alpha \left\| {}^{S}_{E}\dot{\boldsymbol{q}}_{\omega,t} \right\| \Delta t, \ \alpha > 1 \tag{22} $$

C. Algorithm fusion process

In practice, ${}^{S}_{E}\boldsymbol{q}_{\omega,t}$ may start from incorrect initial conditions and acclimate errors due to gyroscope measurement noise and ${}^{S}_{E}\boldsymbol{q}_{\nabla,t}$ will provide an incorrect estimate when the accelerometer is not stationary or the magnetometer exposed to interferences. The goal of the fusion algorithm is to provide an orientation estimate where ${}^{S}_{E}\boldsymbol{q}_{\omega,t}$ is used to filter out high frequency errors in ${}^{S}_{E}\boldsymbol{q}_{\nabla,t}$, and ${}^{S}_{E}\boldsymbol{q}_{\nabla,t}$ is used both to compensate for integral drift in ${}^{S}_{E}\boldsymbol{q}_{\omega,t}$ and to provide convergence from initial conditions.

An estimated orientation of the earth frame relative to the sensor frame, ${}^{S}_{E}\boldsymbol{q}_{est,t}$, is obtained through the fusion of the two separate orientation calculations, ${}^{S}_{E}\boldsymbol{q}_{\omega,t}$ and ${}^{S}_{E}\boldsymbol{q}_{\nabla,t}$ as described by equation (23) where γ_t and $(1 - \gamma_t)$ are weights applied to each orientation calculation.

$$ {}^{S}_{E}\boldsymbol{q}_{est,t} = \gamma_t {}^{S}_{E}\boldsymbol{q}_{\nabla,t} + (1 - \gamma_t) {}^{S}_{E}\boldsymbol{q}_{\omega,t}, \ 0 \leq \gamma_t \leq 1 \tag{23} $$

An optimal value of γ_t is therefore that which ensures the weighted rate of divergence of ${}^S_E\boldsymbol{q}_\omega$ due to integral drift is equal to the weighted rate of convergence of ${}^S_E\boldsymbol{q}_\nabla$. This is represented by equation (24) where $\frac{\mu_t}{\Delta t}$ is the convergence rate of ${}^S_E\boldsymbol{q}_\nabla$ and β is the divergence rate of ${}^S_E\boldsymbol{q}_\omega$ expressed as the magnitude of a quaternion derivative corresponding to the gyroscope measurement error. Equation (24) can be rearranged to define γ_t as equation (25).

$$(1-\gamma_t)\beta = \gamma_t \frac{\mu_t}{\Delta t} \tag{24}$$

$$\gamma_t = \frac{\beta}{\frac{\mu_t}{\Delta t} + \beta} \tag{25}$$

The fusion process ensures the optimal fusion of ${}^S_E\boldsymbol{q}_{\omega,t}$ and ${}^S_E\boldsymbol{q}_{\nabla,t}$ assuming that the convergence rate of ${}^S_E\boldsymbol{q}_\nabla$ governed by α is equal or greater than the physical rate of change of orientation. Therefore α has no upper bound. If α is assumed to be very large then μ_t, defined by equation (22), also becomes very large and the equations simplify. A large value of μ_t used in equation (20) means that ${}^S_E\hat{\boldsymbol{q}}_{est,t-1}$ becomes negligible and the equation can be re-written as equation (26).

$${}^S_E\boldsymbol{q}_{\nabla,t} \approx -\mu_t \frac{\nabla \boldsymbol{f}}{\|\nabla \boldsymbol{f}\|} \tag{26}$$

The definition of γ_t in equation (25) also simplifies if the β term in the denominator becomes negligible and the equation can be rewritten as equation (27). It is possible from equation (27) to also assume that $\gamma_t \approx 0$.

$$\gamma_t \approx \frac{\beta \Delta t}{\mu_t} \tag{27}$$

Substituting equations (4), (26) and (27) into equation (23) directly yields equation (28). It is important to note that in equation (28), γ_t has been substituted as both as equation (26) and 0.

$${}^S_E\boldsymbol{q}_{est,t} = \frac{\beta \Delta t}{\mu_t}\left(-\mu_t \frac{\nabla \boldsymbol{f}}{\|\nabla \boldsymbol{f}\|}\right) + (1-0)\left({}^S_E\hat{\boldsymbol{q}}_{est,t-1} + {}^S_E\dot{\boldsymbol{q}}_{\omega,t}\Delta t\right) \tag{28}$$

Equation (28) can be simplified to equation (29) where ${}^S_E\dot{\boldsymbol{q}}_{est,t}$ is the estimated orientation rate defined by equation (30).

$${}^S_E\boldsymbol{q}_{est,t} = {}^S_E\hat{\boldsymbol{q}}_{est,t-1} + {}^S_E\dot{\boldsymbol{q}}_{est,t}\Delta t \tag{29}$$

$${}^S_E\dot{\boldsymbol{q}}_{est,t} = {}^S_E\dot{\boldsymbol{q}}_{\omega,t} - \beta \frac{\nabla \boldsymbol{f}}{\|\nabla \boldsymbol{f}\|} \tag{30}$$

It can be seen from equations (29) and (30) that the algorithm calculates the orientation ${}^S_E\boldsymbol{q}_{est}$ by numerically integrating the estimated rate of change of orientation ${}^S_E\dot{\boldsymbol{q}}_{est}$. The algorithm computes ${}^S_E\dot{\boldsymbol{q}}_{est}$ as the rate of change of orientation measured by the gyroscopes, ${}^S_E\dot{\boldsymbol{q}}_{\omega}$, with the magnitude of the gyroscope measurement error, β, removed in a direction based on accelerometer and magnetometer measurements. Fig.1 shows a block diagram representation of the complete orientation estimation algorithm implementation for an IMU.

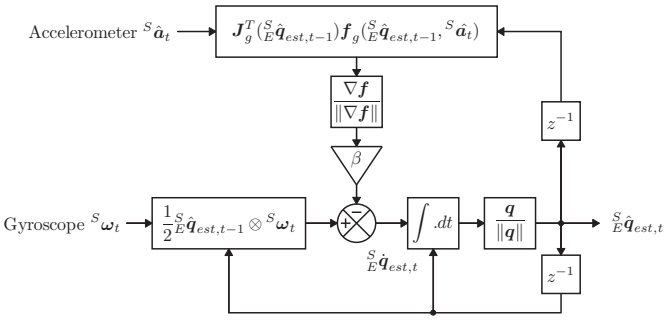

Fig. 1. Block diagram representation of the complete orientation estimation algorithm for an IMU implementation

D. Magnetic distortion compensation

Investigations into the effect of magnetic distortions on an orientation sensor's performance have shown that substantial errors may be introduced by sources including electrical appliances, metal furniture and metal structures within a buildings construction [30], [31]. Sources of interference fixed in the sensor frame, termed hard iron biases, can be removed through calibration [32], [33], [34], [35]. Sources of interference in the earth frame, termed soft iron errors, may only be removed if an additional reference of orientation is available. An accelerometer provides a reference of attitude and so may be used to compensate for inclination errors in the measured earth's magnetic field.

The measured direction of the earth's magnetic field in the earth frame at time t, ${}^E\hat{\boldsymbol{h}}_t$, can be computed as equation (31). The effect of an erroneous inclination of the measured direction earth's magnetic field, ${}^E\hat{\boldsymbol{h}}_t$, can be corrected if the algorithm's reference direction of the earth's magnetic field, ${}^E\hat{\boldsymbol{b}}_t$, is of the same inclination. This is achieved by computing ${}^E\hat{\boldsymbol{b}}_t$ as ${}^E\hat{\boldsymbol{h}}_t$ normalised to have only components in the earth frame x and z axes; as described by equation (32).

$${}^E\hat{\boldsymbol{h}}_t = \begin{bmatrix} 0 & h_x & h_y & h_z \end{bmatrix} = {}^S_E\hat{\boldsymbol{q}}_{est,t-1} \otimes {}^S\hat{\boldsymbol{m}}_t \otimes {}^S_E\hat{\boldsymbol{q}}^*_{est,t-1} \tag{31}$$

$${}^E\hat{\boldsymbol{b}}_t = \begin{bmatrix} 0 & \sqrt{h_x^2 + h_y^2} & 0 & h_z \end{bmatrix} \tag{32}$$

Compensating for magnetic distortions in this way ensures that magnetic disturbances are limited to only affect the estimated heading component of orientation. The approach also eliminates the need for the reference direction of the earth's magnetic field to be predefined; a potential disadvantage of other orientation estimation algorithm [12], [19]. Fig.2 shows a block diagram representation of the complete algorithm implementation for a MARG sensor array, including the magnetic distortion compensation.

E. Algorithm adjustable parameter

The orientation estimation algorithm requires 1 adjustable parameter, β, representing the gyroscope measurement error expressed as the magnitude of a quaternion derivative. It is convenient to define β using the angular quantity $\tilde{\omega}_{max}$

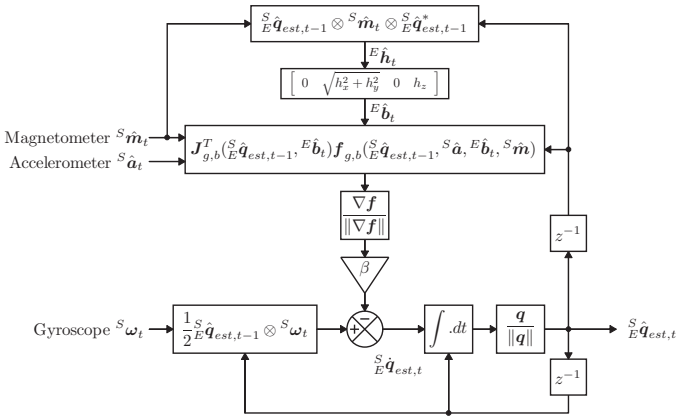

Fig. 2. Block diagram representation of the complete orientation estimation algorithm for an MARG implementation including magnetic distortion compensation

representing the maximum gyroscope measurement error of each axis. Using the relationship described by equation (2), β may be defined by equation (33) where $\hat{\boldsymbol{q}}$ is any unit quaternion.

$$\beta = \left\| \frac{1}{2}\hat{\boldsymbol{q}} \otimes \begin{bmatrix} 0 & \tilde{\omega}_{max} & \tilde{\omega}_{max} & \tilde{\omega}_{max} \end{bmatrix} \right\| = \sqrt{\frac{3}{4}}\tilde{\omega}_{max} \quad (33)$$

IV. Experimental Equipment

The algorithm was tested using the xsens MTx orientation sensor [13] containing 16 bit resolution tri-axis gyroscopes, accelerometers and magnetometers. Raw sensor data was logged to a PC at 512 Hz and imported accompanying software to provide calibrated sensor measurements which were then processed by the proposed orientation estimation algorithm. The software also incorporates a propriety Kalman-based orientation estimation algorithm. As both the Kalman-based algorithm and proposed algorithm's estimates of orientation were computed using identical sensor data, the performance of each algorithm could be evaluated relative to one-another, independent of sensor performance.

A Vicon system, consisting of 8 MX3+ cameras connected to an MXultranet server [36] and Nexus [37] software, was used to provide reference measurements of the orientation sensor's actual orientation. To do so, the sensor was fixed to an orientation measurement platform. The positions of optical markers attached to the platform were logged at 120 Hz and then post-processed to compute the orientation of the measurement platform and sensor. In order for the measurements of an orientation in the camera coordinate frame to be comparable to the algorithm estimate of orientation in the earth frame, an initial calibration procedure was required where the direction of the earth's magnetic and gravitational fields in the camera coordinate frame were measured using a magnetic compass and pendulum with attached optical markers.

V. Experimental Results

It is common [19], [21], [13], [14], [15], [16] to quantify orientation sensor performance as the static and dynamic RMS

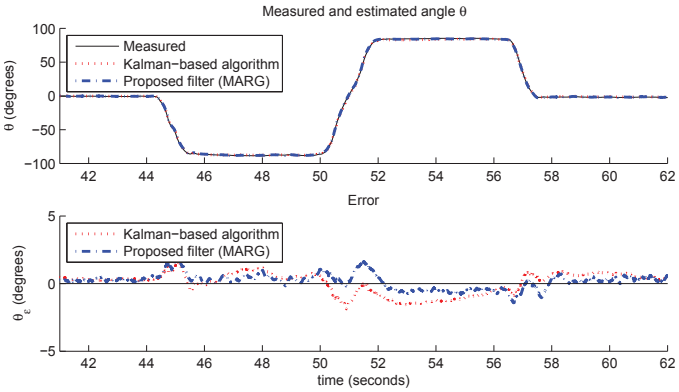

Fig. 3. Typical results for measured and estimated angle θ (top) and error (bottom)

TABLE I
Static and dynamic RMS error of Kalman-based algorithm and proposed algorithm IMU and MARG implementations

Euler parameter	Kalman-based algorithm	MARG algorithm	IMU algorithm
RMS$[\phi_\epsilon]$ static	0.789°	0.581°	0.594°
RMS$[\phi_\epsilon]$ dynamic	0.769°	0.625°	0.623°
RMS$[\theta_\epsilon]$ static	0.819°	0.502°	0.497°
RMS$[\theta_\epsilon]$ dynamic	0.847°	0.668°	0.668°
RMS$[\psi_\epsilon]$ static	1.150°	1.073°	N/A
RMS$[\psi_\epsilon]$ dynamic	1.344°	1.110°	N/A

(Root-Mean-Square) errors in the decoupled Euler parameters describing the pitch, ϕ, roll, θ and heading, ψ components of an orientation, corresponding to rotations around the sensor frame x, y, and z axis respectively. A total of 4 sets of Euler parameters were computed, corresponding to the calibrated optical measurements of orientation, the Kalman-based algorithm estimated orientation and the proposed algorithm estimates orientation for both the MARG and IMU implementations. The errors of estimated Euler parameters, ϕ_ϵ, θ_ϵ and ψ_ϵ, were computed as the difference between estimated values and the calibrated optical measurements. Results were obtained for a sequence of rotations around each axis preformed by hand. The experiment was repeated 8 times to compile a dataset representative of system performance. The proposed algorithm's adjustable parameter, β, was set to 0.033 for the MARG implementation and 0.041 for the IMU implementation. Trials summarised in Fig.4, found these values to provide optimal performance. Fig.3 shows the Kalman-based algorithm and proposed algorithm MARG implementation results, typical of the 8 experiments.

The static and dynamic RMS values of ϕ_ϵ, θ_ϵ, and ψ_ϵ were calculated assuming a static state when the measured corresponding angular rate was $< 5^\circ/\text{s}$, and a dynamic when $\geq 5^\circ/\text{s}$. This threshold was chosen to be sufficiently greater than the noise floor of the data. The results are summarised in Table I where each value, represents the mean of all 8 experiments.

The results of an investigation into the effect of the adjustable parameter β on algorithm performance are summarised in Fig.4. The experimental data was processed though the separate proposed algorithm IMU and MARG implanta-

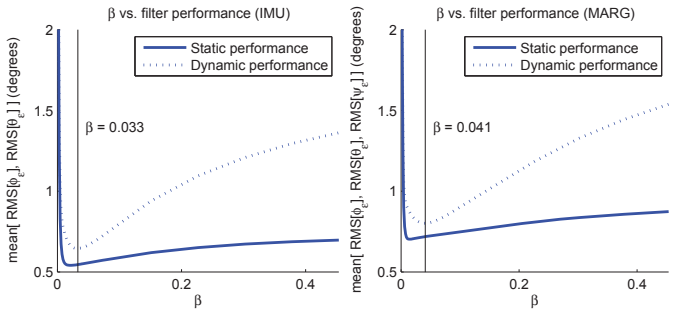

Fig. 4. The effect of the adjustable parameter, β, on the performance of the proposed algorithm IMU (left) and MARG (right) implementations

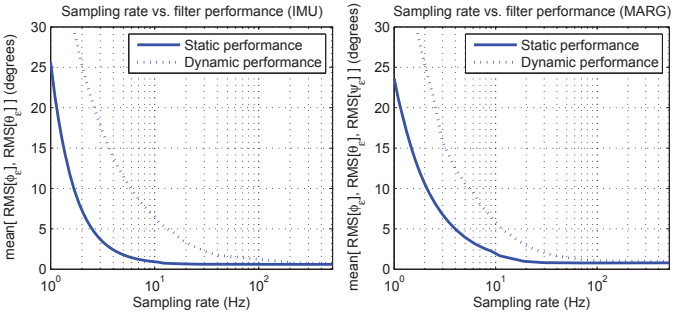

Fig. 5. The effect of sampling rate on the performance of the proposed algorithm IMU (left) and MARG (right) implementations

tions, using fixed values of β between 0 to 0.5. There is a clear optimal value of β high enough to minimises errors due to integral drift but sufficiently low enough that unnecessary noise is not introduced by large steps of gradient descent iterations.

The results of an investigation into the effect of sampling rate on algorithm performance is summarised in Fig.5. The experimental data was processed though the separate proposed algorithm IMU and MARG implantations, using the previously defined, optimal values β. Experimental data was decimated to simulate sampling rates between 1Hz and 512 Hz. It can be seen from Fig.5 that the proposed algorithm achieves similar levels of performance at 50 Hz as at 512 Hz. Both algorithm implementations are able to achieve a static error $< 2°$ and dynamic error $< 7°$ while sampling at 10 Hz. This level of accuracy may be sufficient for human motion applications though the sampling rate will limit the bandwidth of the motion that may be measured.

VI. Conclusions

Orientation estimation algorithms for inertial/magnetic sensors is a is a mature field of research. Modern techniques [25], [26], [38] have focused on simpler algorithms that ameliorate the computational load and parameter tuning burdens associated with conventional Kalman-based approaches. The algorithm presented in this paper employs processes similar to others but through a novel derivation, is able to offer some key advantages:

- Computing an error based on an analytically derived Jacobian results in a significant reduction in the computation load relative to a Gauss-Newton method [25]; quantified as 109 and 248 scalar arithmetic operations per update for C code implementations of the IMU and MARG implementations respectively.
- Normalisation of the feedback error permits optimal gains to be defined based on observable system characteristics.
- Magnetic distortion compensation algorithm eliminates the need for a direction of magnetic field to be predefined by the designer.

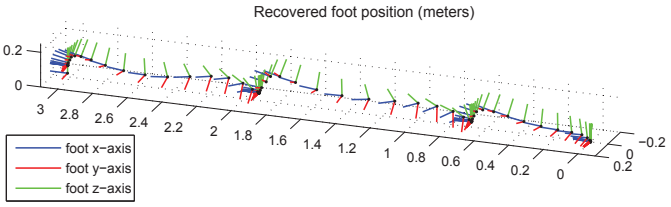

Fig. 6. Recovered foot position plotted at 20 samples per second

The elimination of a predefined direction of magnetic field is an advantage over all other algorithms cited by this paper; though this component may be easily incorporated to other algorithms. Experimental studies have been presented for an off-the-shelf, leading commercial unit with reference measurements obtained via precision optical measurement system. These studies enabled the algorithm to be benchmarked and have indicated that the algorithm performs as well as the proprietary Kalman-based system; even with a full order of magnitude in reduction of sampling rate.

VII. Future work

Research is presently underway to incorporate the orientation estimation algorithm into a self-contained human motion tracking system for rehabilitative applications. As stated earlier, Zhoua [7] cited real time operation, wireless properties, correctness of data, and portability as major challenges to be addressed. The reduction in computational load and relative ease in tuning provided by the algorithm introduced in this work addresses all of these issues; its efficiency allows implementation on low power, low performance, hardware for significant reduction in size, while its sampling rates permits longer periods of data storage and simpler implementation for wireless data transfer.

The algorithm is currently being implemented as the core of a self-contained system with a MARG suite, data storage unit, and power supply that will be small enough to fit within the sole of a sports shoe for lower extremity motion tracking. Fig.6 shows data obtained using a prototype unit for tracking of the right foot of a test subject as they walked in a straight line. Translational position data was recovered using methods similar to [39], [40], [41], [42], [43]. The measured distance of the 3 steps was 3.0 m, while the recovered displacement was 3.00 m. A complete system is currently under development to allow long-term (1 week +) motion tracking in unstructured environments.

REFERENCES

[1] S. K. Hong, "Fuzzy logic based closed-loop strapdown attitude system for unmanned aerial vehicle (uav)," *Sensors and Actuators A: Physical*, vol. 107, no. 2, pp. 109 – 118, 2003.

[2] B. Barshan and H. F. Durrant-Whyte, "Inertial navigation systems for mobile robots," vol. 11, pp. 328–342, June 1995.

[3] L. Ojeda and J. Borenstein, "Flexnav: fuzzy logic expert rule-based position estimation for mobile robots on rugged terrain," in *Proc. IEEE International Conference on Robotics and Automation ICRA '02*, vol. 1, pp. 317–322, May 11–15, 2002.

[4] D. H. Titterton and J. L. Weston, *Strapdown inertial navigation technology*. The Institution of Electrical Engineers, 2004.

[5] S. Beauregard, "Omnidirectional pedestrian navigation for first responders," in *Proc. 4th Workshop on Positioning, Navigation and Communication WPNC '07*, pp. 33–36, Mar. 22–22, 2007.

[6] H. J. Luinge and P. H. Veltink, "Inclination measurement of human movement using a 3-d accelerometer with autocalibration," vol. 12, pp. 112–121, Mar. 2004.

[7] H. Zhou and H. Hu, "Human motion tracking for rehabilitation–a survey," *Biomedical Signal Processing and Control*, vol. 3, no. 1, pp. 1 – 18, 2008.

[8] E. A. Heinz, K. S. Kunze, M. Gruber, D. Bannach, and P. Lukowicz, "Using wearable sensors for real-time recognition tasks in games of martial arts - an initial experiment," in *Proc. IEEE Symposium on Computational Intelligence and Games*, pp. 98–102, May 22–24, 2006.

[9] R. E. Kalman, "A new approach to linear filtering and prediction problems," *Journal of Basic Engineering*, vol. 82, pp. 35–45, 1960.

[10] E. Foxlin, "Inertial head-tracker sensor fusion by a complementary separate-bias kalman filter," in *Proc. Virtual Reality Annual International Symposium the IEEE 1996*, pp. 185–194,267, Mar. 30–Apr. 3, 1996.

[11] H. J. Luinge, P. H. Veltink, and C. T. M. Baten, "Estimation of orientation with gyroscopes and accelerometers," in *Proc. First Joint [Engineering in Medicine and Biology 21st Annual Conf. and the 1999 Annual Fall Meeting of the Biomedical Engineering Soc.] BMES/EMBS Conference*, vol. 2, p. 844, Oct. 13–16, 1999.

[12] J. L. Marins, X. Yun, E. R. Bachmann, R. B. McGhee, and M. J. Zyda, "An extended kalman filter for quaternion-based orientation estimation using marg sensors," in *Proc. IEEE/RSJ International Conference on Intelligent Robots and Systems*, vol. 4, pp. 2003–2011, Oct. 29–Nov. 3, 2001.

[13] Xsens Technologies B.V., *MTi and MTx User Manual and Technical Documentation*. Pantheon 6a, 7521 PR Enschede, The Netherlands, May 2009.

[14] MicroStrain Inc., *3DM-GX3 -25 Miniature Attutude Heading Reference Sensor*. 459 Hurricane Lane, Suite 102, Williston, VT 05495 USA, 1.04 ed., 2009.

[15] VectorNav Technologies, LLC, *VN -100 User Manual*. College Station, TX 77840 USA, preliminary ed., 2009.

[16] InterSense, Inc., *InertiaCube2+ Manual*. 36 Crosby Drive, Suite 150, Bedford, MA 01730, USA, 1.0 ed., 2008.

[17] PNI sensor corporation, *Spacepoint Fusion*. 133 Aviation Blvd, Suite 101, Santa Rosa, CA 95403-1084 USA.

[18] Crossbow Technology, Inc., *AHRS400 Series Users Manual*. 4145 N. First Street, San Jose, CA 95134, rev. c ed., February 2007.

[19] A. M. Sabatini, "Quaternion-based extended kalman filter for determining orientation by inertial and magnetic sensing," vol. 53, pp. 1346–1356, July 2006.

[20] H. J. Luinge and P. H. Veltink, "Measuring orientation of human body segments using miniature gyroscopes and accelerometers," *Medical and Biological Engineering and Computing*, vol. 43, pp. 273–282, April 2006.

[21] D. Jurman, M. Jankovec, R. Kamnik, and M. Topic, "Calibration and data fusion solution for the miniature attitude and heading reference system," *Sensors and Actuators A: Physical*, vol. 138, pp. 411–420, August 2007.

[22] M. Haid and J. Breitenbach, "Low cost inertial orientation tracking with kalman filter," *Applied Mathematics and Computation*, vol. 153, pp. 567–575, June 2004.

[23] D. Roetenberg, H. J. Luinge, C. T. M. Baten, and P. H. Veltink, "Compensation of magnetic disturbances improves inertial and magnetic sensing of human body segment orientation," vol. 13, pp. 395–405, Sept. 2005.

[24] R. A. Hyde, L. P. Ketteringham, S. A. Neild, and R. J. S. Jones, "Estimation of upper-limb orientation based on accelerometer and gyroscope measurements," vol. 55, pp. 746–754, Feb. 2008.

[25] E. R. Bachmann, R. B. McGhee, X. Yun, and M. J. Zyda, "Inertial and magnetic posture tracking for inserting humans into networked virtual environments," pp. 9–16, 2001.

[26] R. Mahony, T. Hamel, and J.-M. Pflimlin, "Nonlinear complementary filters on the special orthogonal group," *Automatic Control, IEEE Transactions on*, vol. 53, pp. 1203 –1218, june 2008.

[27] J. J. Craig, *Introduction to Robotics Mechanics and Control*. Pearson Education International, 2005.

[28] D. R. P. R. B. M. Joseph M. Cooke, Michael J. Zyda, "Npsnet: Flight simulation dynamic modelling using quaternions," *Presence*, vol. 1, pp. 404–420, 1994.

[29] J. A. Jacobs, *The earth's core*, vol. 37 of International geophysics series. Academic Press, 2 ed., 1987.

[30] E. R. Bachmann, X. Yun, and C. W. Peterson, "An investigation of the effects of magnetic variations on inertial/magnetic orientation sensors," in *Proc. IEEE International Conference on Robotics and Automation ICRA '04*, vol. 2, pp. 1115–1122, Apr. 2004.

[31] C. B. F. v. d. H. W.H.K. de Vries, H.E.J. Veeger, "Magnetic distortion in motion labs, implications for validating inertial magnetic sensors," *Gait & Posture*, vol. 29, no. 4, pp. 535–541, 2009.

[32] Speake & Co Limited, "Autocalibration algorithms for FGM type sensors." Application note.

[33] M. J. Caruso, *Applications of Magnetoresistive Sensors in Navigation Systems*. Honeywell Inc., Solid State Electronics Center, Honeywell Inc. 12001 State Highway 55, Plymouth, MN 55441.

[34] J. F. Vasconcelos, G. Elkaim, C. Silvestre, P. Oliveira, and B. Cardeira, "A geometric approach to strapdown magnetometer calibration in sensor frame," in *Navigation, Guidance and Control of Underwater Vehicles*, vol. 2, 2008.

[35] D. Gebre-Egziabher, G. H. Elkaim, J. D. Powell, and B. W. Parkinson, "Calibration of strapdown magnetometers in magnetic field domain," *Journal of Aerospace Engineering*, vol. 19, no. 2, pp. 87–102, 2006.

[36] Vicon Motion Systems Limited., *Vicon MX Hardware*. 5419 McConnell Avenue, Los Angeles, CA 90066, USA, 1.6 ed., 2004.

[37] Vicon Motion Systems Limited., *Vicon Nexus Product Guide - Foundation Notes*. 5419 McConnell Avenue, Los Angeles, CA 90066, USA, 1.2 ed., November 2007.

[38] P. Martin and E. Salan, "Design and implementation of a low-cost observer-based attitude and heading reference system," *Control Engineering Practice*, vol. 18, no. 7, pp. 712 – 722, 2010. Special Issue on Aerial Robotics.

[39] X. Yun, E. R. Bachmann, H. Moore, and J. Calusdian, "Self-contained position tracking of human movement using small inertial/magnetic sensor modules," in *ICRA*, pp. 2526–2533, 2007.

[40] E. Foxlin, "Pedestrian tracking with shoe-mounted inertial sensors," *IEEE Comput. Graph. Appl.*, vol. 25, no. 6, pp. 38–46, 2005.

[41] H. M. Schepers, H. Koopman, and P. H. Veltink, "Ambulatory assessment of ankle and foot dynamics," *IEEE Transactions on Biomedical Engineering*, vol. 54, no. 5, pp. 895–902, 2007.

[42] R. Stirling, K. Fyfe, and G. Lachapelle, "Evaluation of a new method of heading estimation for pedestrian dead reckoning using shoe mounted sensors," *The Journal of Navigation*, vol. 58, no. 01, pp. 31–45, 2005.

[43] F. Cavallo, A. Sabatini, and V. Genovese, "A step toward gps/ins personal navigation systems: real-time assessment of gait by foot inertial sensing," pp. 1187 – 1191, aug. 2005.